applied sciences

Article

Research on Unsteady Burgers Creep Constitutive Model and Secondary Development Application

Ruonan Zhu [1,*], Bo Wu [2], Shixiang Xu [2], Xi Liu [3] and Heshan Li [3]

[1] School of Water Resources and Environmental Engineering, East China University of Technology, Nanchang 330013, China
[2] School of Civil and Architecture Engineering, East China University of Technology, Nanchang 330013, China
[3] China Tielong Engineering Group Co., Ltd., Chendu 610000, China
* Correspondence: zhurn96@163.com

Abstract

Considering the complexity and diversity of water-rich soft soil strata, indoor triaxial shear tests and creep tests were conducted on soft soil to explore its deformation law and creep characteristics. To address the nonlinear characteristics of soft soil creep, a nonlinear pot element was proposed and substituted for the two linear pot elements in the Burgers model, thus establishing an unsteady parametric Burgers model. The one-dimensional creep equation of the unsteady Burgers model was derived, theoretically determining that the unsteady model can describe three stages of creep. Based on this, the creep equation of the unsteady Burgers model was extended to a three-dimensional stress state, and the triaxial compression creep test curves of Ningbo soft soil were fitted and parameters identified. The above model was derived from a three-dimensional finite difference scheme suitable for numerical solution in FLAC3D. A custom constitutive creep model was developed in FLAC3D, and the non-accelerated creep stage and accelerated creep stage of the improved model were analyzed to verify the accuracy and reliability of the constitutive model. The results show that the numerical simulation results and the indoor creep test results are in good agreement in terms of strain increment and the creep change curve, which confirms the effectiveness and applicability of the proposed unsteady Burgers creep constitutive model and its secondary development application.

Keywords: soft soil creep; unsteady Burgers model; three-dimensional creep equation; parameter identification; secondary development

Academic Editor: Jordi Puiggali

Received: 2 December 2025
Revised: 18 December 2025
Accepted: 29 December 2025
Published: 30 December 2025

1. Introduction

With the acceleration of urbanization, the utilization rate of urban underground space has increased year by year. During construction, water-rich soft soil strata often exhibit more nonlinearity and time dependence [1,2]. Among them, the soil is gradually deformed by construction disturbance over time. Its creep deformation will lead to uneven stress on the support structure of underground engineering, causing excessive deformation, instability, or even collapse. Nonlinear creep constitutive models can more accurately reflect the complex process of soil creep, thereby truly assessing the construction stability of underground engineering and providing a guarantee for engineering safety. FLAC3D 6.0 numerical software has many classic creep constitutive models built in, but it cannot meet the soil creep situation under complex geological conditions [3–5], which makes the soil deformation simulation more idealized and different from the actual situation and cannot accurately analyze the structural stability judgment in engineering construction. Therefore, according to the different hydrogeological conditions of the project, establishing a targeted creep constitutive model is a necessary means to improve and perfect the creep analysis of rock and soil [6–8], which helps to improve the accuracy of structural deformation prediction and the overall safety of the project.

Traditional creep models are formed by a combination of linear elements, which can reflect the decay creep stage and the steady-state creep stage but cannot reflect the accelerated creep stage. Therefore, many researchers have constructed nonlinear creep models to study the three stages of creep in soil and rock. Researchers [9–13] have connected nonlinear viscoplastic elements with traditional viscoelastic creep models for soil and rock with different properties to form corresponding nonlinear viscoelastic–plastic creep models. Verification studies have shown that they can all meet the three-stage characteristic analysis of creep deformation in soil and rock. Sterpi et al. [14] connected a viscoplastic element in series with the Kelvin–Voigt model to construct a nonlinear viscoelastic–plastic creep model. Based on the fact that the Sterpi model cannot accurately predict steady-state creep under low-stress conditions, Fahimifar et al. [15] proposed to connect a plastic element that satisfies the Mohr–Coulomb criterion in series on this model. The results showed that the new creep model can accurately predict steady-state creep under low stress. Yin et al. [16] made a nonlinear improvement to the Burgers model, constructing a hard rock nonlinear creep constitutive model considering damage and inverting and verifying the model parameters. Jiang [17] et al. considered time-dependent damage in the creep process, derived a three-dimensional nonlinear creep model, and compared the numerical simulation results with the experimental results; Tang Zhiqiang [18] and Li Zhongjun [19] et al., based on considering time-dependent damage, introduced time-triggered elements, established a creep damage model, and carried out parameter identification and verification. In order to accurately simulate the creep process of rock and soil in engineering practice, researchers have carried out secondary development of the creep constitutive model built into FLAC3D to solve the nonlinear creep problem of different rock and soil. Chen et al. [20] improved the Poynting–Thomson creep model based on damage theory and carried out the secondary development of the improved creep model using C++ language and FLAC3D built-in Fish language. Zhu Xin et al. [21] proposed a viscoelastic–plastic element that can reflect the accelerated rheological properties of rocks and connected it in series with the traditional Burgers model. They then embedded the improved Burgers model into FLAC3D for development and application. Adding more element parameters to the traditional model can accurately describe the creep process of soil and rock, but it is difficult to calculate, and it is difficult to accurately present the complex model in numerical software. Therefore, it is crucial to select simplified unsteady parameters and form a nonlinear creep constitutive model for the specific characteristics of soil and rock.

Based on this, this paper conducts indoor triaxial shear tests and triaxial creep tests on soft soil to analyze the influence of these tests on soil properties. A nonlinear Burgers creep model is constructed based on the indoor test data; its one-dimensional creep equation is derived and extended to the three-dimensional stress state. The improved model is further developed using C++ language and FLAC3D numerical software, providing an analytical method for more accurate analysis of creep deformation in complex soft soil.

2. Triaxial Creep Test Analysis of Soft Soil

2.1. Test Materials

In the construction of water-rich soft soil strata in Ningbo, there are many soil layers. Based on the engineering geological conditions, the soil layers in the project area and the area of influence are mostly silty clay. This type of soil is relatively soft and has strong

https://doi.org/10.3390/app16010424

creep. Therefore, this experiment selected this type of soil for sample preparation. The samples were taken from the foundation pit construction site of a subway station in Ningbo using a thin-walled sampler. The sampling site and soil samples are shown in Figure 1. The relevant physical and mechanical parameters of the soil samples were determined according to the "Standard for Geotechnical Testing Methods" (GB/T 50123-2019) [22], including water content ω, density ρ, and permeability coefficient *k*. Thirty soil samples were taken from the required depth to carry out physical mechanical tests. The average value of the soil sample test is obtained to obtain the final standard value of physical and mechanical parameters, as shown in Table 1.

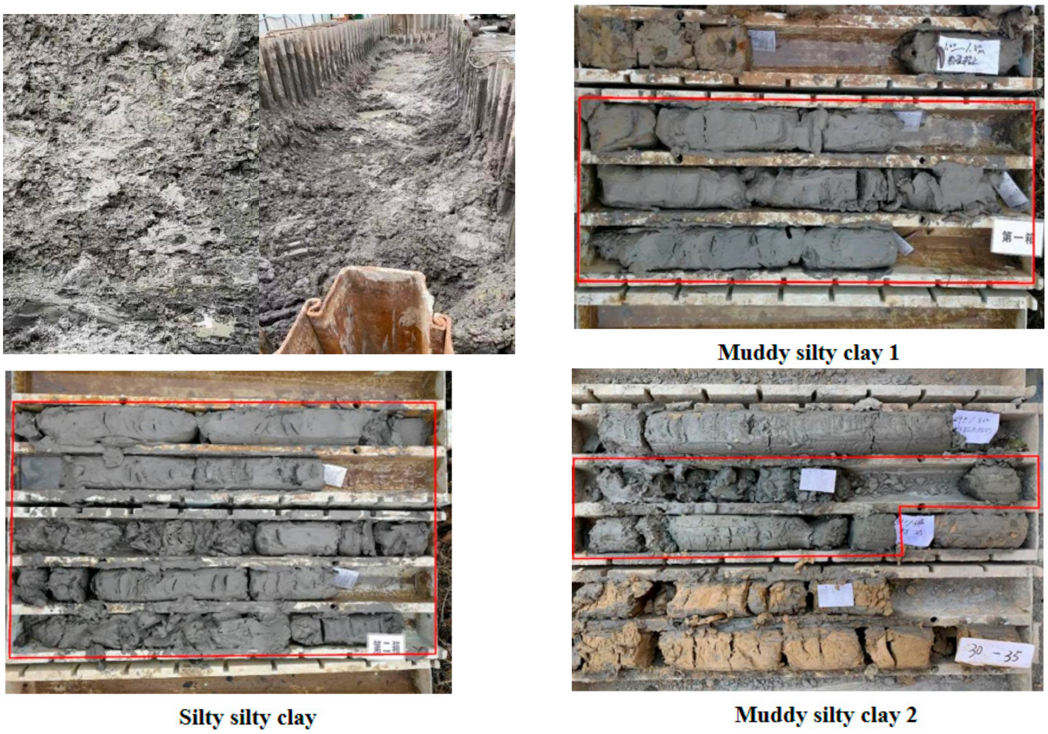

Figure 1. Sampling and sampling site.

Table 1. Standard values of physical and mechanical parameters of soft soil.

Soil Sample Name	Muddy Silty Clay 1	Silty Silty Clay	Muddy Silty Clay 2
Sampling depth h (m)	8	12	20
Natural density ρ (g/cm^3)	1.75	1.93	1.78
Cohesion c (kPa)	12.5	13	13.6
Angle of friction φ (°)	13.7	16	14.8
Elastic modulus E (MPa)	26	25	20
Poisson's ratio ν	0.35	0.29	0.35
Permeability coefficient k (cm/s)	3.79×10^{-7}	5.71×10^{-7}	6.58×10^{-7}
Moisture content ω (%)	45.9	45.3	46.1
Saturation Sr (%)	40.5	31.8	39.6
Void ratio e	0.995	0.645	1.006

2.2. Test Equipment and Scheme

The instrument required for the test was an MTS servo hydraulic fatigue testing machine, as shown in Figure 2. Triaxial shear tests and creep tests were conducted. The loading and unloading of the specimens were controlled according to the set program during the test. The equipment is highly stable and can work for a long time, and the data collected is accurate and stable.

Figure 2. MTS servo hydraulic fatigue testing machine.

Based on the engineering conditions, this paper explores the influence of creep on the deformation of foundation pit construction. The permeability coefficient of the three-layer soil is small (10^{-6} secondary), and dewatering will be carried out during the excavation of the foundation pit. Therefore, a triaxial undrained creep test was selected. The test soil sample is saturated, and the pore water is incompressible. Therefore, the triaxial undrained creep test is selected, and the test temperature is controlled at 20 ± 2 °C.

(1) To ensure the soil structure of the foundation pit project is not disturbed excessively, this test uses undisturbed soil for the experimental study. The sample size is 50 mm × 100 mm. Three samples are selected in each group of tests, and the average value of the test results of the three samples is taken. In order to ensure the uniformity of stress distribution at the end of the test, friction gaskets are placed on the upper and lower end of the soil sample.
(2) A triaxial consolidated undrained test was conducted on the specimen. The confining pressure of the conventional triaxial consolidated undrained shear test was applied by the actual small principal stress $\sigma_3 = K_0 \sum \gamma_i h_i$ of the soil (γ_i is the soil density, K_0 is the soil pressure coefficient, and $K_0 = 1 - \sin\phi$. The strain-controlled loading method is adopted, the shear rate is set to 0.07 mm min, and the test is terminated when the cumulative axial strain reaches 16%.
(3) A triaxial undrained creep test is performed on the specimen, a certain confining pressure is kept constant, and then deviatoric stress q is applied. Approximately 80% of the ultimate deviatoric stress obtained from the triaxial undrained shear test is taken as the maximum deviatoric stress applied in the creep test [22], and the loading coefficient of the triaxial creep test is 0.3. When the soil sample is destroyed or the test time reaches 12,000 min, the creep test stops.

The confining pressure of the three soil layers is close to 200 kPa, so in the subsequent test, the confining pressure level can be selected according to less than 200 kPa, equal to 200 kPa and greater than 200 kPa, and can be taken as 100 kPa, 200 kPa, and 300 kPa, respectively. In this way, the creep characteristics of the soil under different confining pressure conditions can be compared and studied, and the creep characteristics of the specimen under the actual engineering confining pressure under the test conditions can also be considered.

2.3. Triaxial Consolidated Undrained Shear Test

To obtain the loading range of the creep test, a conventional triaxial undrained shear test was conducted before the creep test to determine the ultimate deviatoric stress of the specimen under different confining pressures.

The stress–strain relationship curves of soil specimens were obtained by triaxial shear test, as shown in Figure 3. With the increase in axial strain, the bias stress increases continuously, and the change trend of bias stress is consistent with the difference in perimeter pressure. At the beginning of the test, the bias stress–strain relationship curve of soft soil was linear, and then, with the increase in axial strain, the bias stress increased at a decreasing rate, but it still increased slowly until the axial strain reached the set value to stop the test. In addition, it can be found in Figure 3 that the larger the perimeter pressure is, the more obvious the hardening and deformation characteristics of the soil body are.

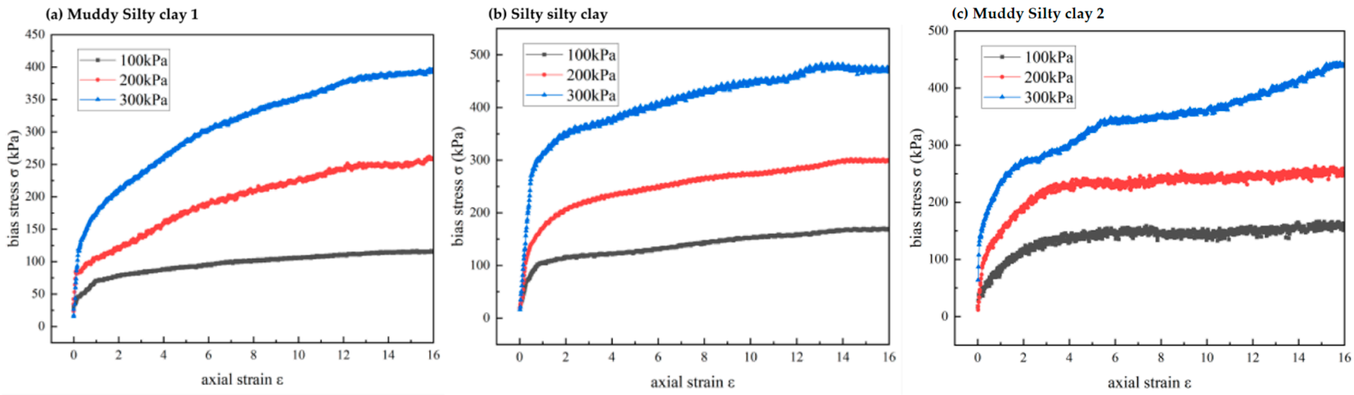

Figure 3. Typical triaxial shear stress–strain relationship curve of soft soil.

Observing the results of the triaxial shear test, see Figure 4, the soil specimens were subjected to a triaxial consolidation undrained shear test. The soil skeleton was subjected to shear dilatancy, but the negative pore water pressure was generated due to being undrained, which led to the increase in effective stress of the soil mass. At the same time, the structural reorganization of the soil skeleton accompanied by instantaneous volume expansion showed a shear dilatation failure mode. The ultimate deviatoric stress obtained from the conventional triaxial shear undrained test of the soil sample is shown in Table 2.

Figure 4. Failure mode of soil sample.

Table 2. Ultimate bias stress of soil mass.

Ultimate Deviatoric Stress q_f (kPa)		Muddy Silty Clay 1	Silty Silty Clay	Muddy Silty Clay 2
confining pressure	100 kPa	116.1	170.3	164.4
	200 kPa	260.8	300.5	259.3
	300 kPa	395.3	475.4	443.4

2.4. Triaxial Consolidation Undrained Creep Test

A triaxial undrained shear creep test was performed on the soil sample. A certain confining pressure was kept constant. Deviatoric stress q was applied by a graded loading method. The stress–strain–time relationship was analyzed. Approximately 80% of the ultimate deviatoric stress obtained from the conventional triaxial undrained shear test was taken as the maximum deviatoric stress applied in the creep test. The deviatoric stress was applied in three levels. The deformation of less than 0.01 mm within 24 h of the creep test was regarded as a sign that the soil reached stability under this stress state. Then, the next level of load was applied [23]. The specific stress application scheme of the creep test is shown in Table 3.

Table 3. Creep test stress application scheme.

Soil Sample	Number	Pre-Consolidation Pressure (kPa)	Creep Confining Pressure (kPa)	Maximum Deviatoric Stress q_f (kPa)	Deviatoric Stress q (kPa)		
Muddy Silty Clay 1	A1	97.1	100	92.9	30	60	90
	A2	187.2	200	208.6	90	140	190
	A3	297.6	300	316.2	140	220	300
Silty Silty Clay	B1	127.4	100	136.2	60	90	120
	B2	220.9	200	240.4	70	140	210
	B3	355.2	300	380.3	120	240	360
Muddy Silty Clay 2	C1	108.4	100	131.6	60	90	120
	C2	201.2	200	207.4	90	140	190
	C3	323.5	300	346.7	140	220	300

Triaxial undrained creep tests are carried out on the soil samples, respectively, and the confining pressure settings are the same as those of the triaxial consolidated undrained shear test (100 kPa, 200 kPa, and 300 kPa, respectively). Subsequently, according to the test results, the triaxial creep time–strain curves of the three soil samples are obtained, as shown in Figure 5. It can be seen from the figure that, with the increase in time, the strain value of soft soil increases continuously, and the creep characteristics are obvious.

As shown in Figure 5, under the same conditions, the greater the confining pressure, the smaller the creep deformation of soft soil. For muddy silty clay and silty silty clay, the deformation of the soil samples increases continuously with time, and the greater the deviatoric stress, the greater the creep deformation, indicating that all three soil samples exhibit a relatively significant creep effect. The greater the deviatoric stress, the greater the initial creep deformation of the soil, while the greater the confining pressure, the smaller the initial deformation of the soil. Taking muddy silty clay 2 as an example, with constant confining pressure, the creep deformation increases by 25~35% with each increase in deviatoric stress, while the creep deformation decreases by 15~25% with each increase of 100 kPa in confining pressure. Furthermore, when the confining pressure and deviatoric stress are both 300 kPa, the sample exhibits an accelerated creep stage, and the soil sample fails after 135 h, with a creep rate of 14.8%. This is because the creep loading coefficient is constant, and the higher the confining pressure, the faster the soil sample undergoes compression consolidation, thus reducing the amount of creep deformation in the sample.

Soil undergoes creep under long-term load. Tests generally show that shear creep is divided into two types: decaying creep and non-decaying creep. The characteristic of decaying creep is that the material deformation rate first increases and then decreases with time, eventually becoming constant. Decaying creep typically exhibits two stages: the decaying creep stage and the steady-state creep stage, as shown in Figure 6. In the early stage, creep develops rapidly, but the deformation gradually weakens. After decreasing to a certain level, the creep rate tends to zero. Although creep is still occurring, it is already in a steady-state creep. Non-decaying creep, after the decaying creep stage and a brief steady-state creep stage, enters an accelerated creep stage, as shown in Figure 6. As time increases, soil creep enters a steady-state development. When the deviatoric stress level reaches a certain critical value, the strain rate increases, and creep enters the accelerated creep stage, at which point the soil will quickly fail.

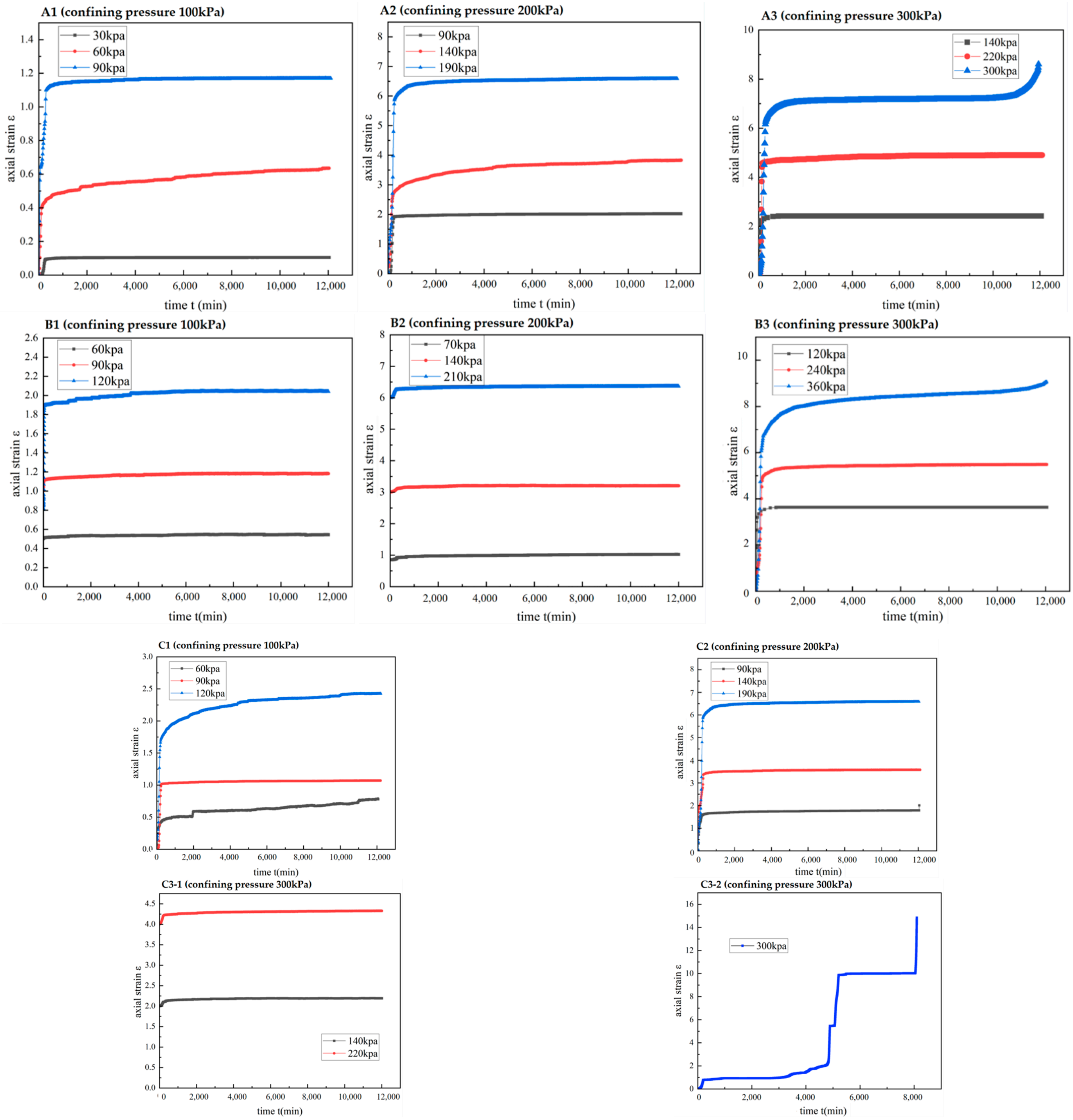

Figure 5. Creep law of soft soil under different confining pressures.

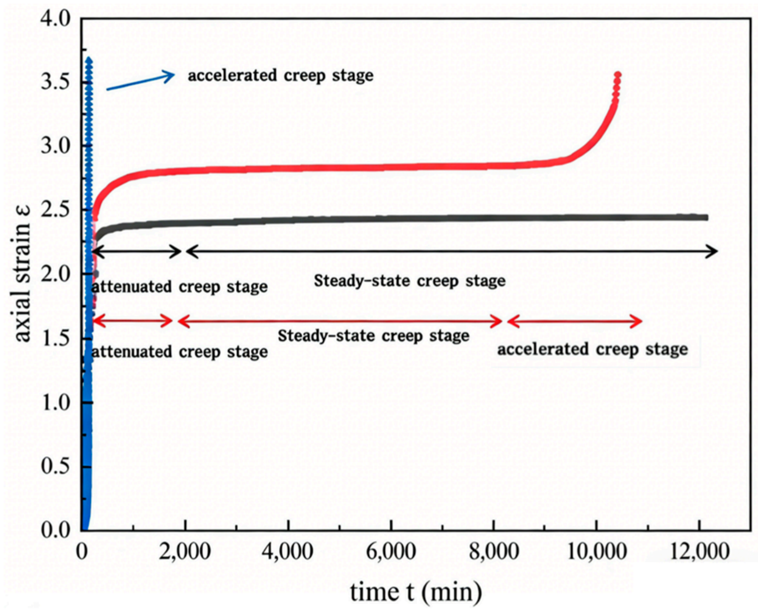

Figure 6. Typical creep curves of soft soil at different creep stages.

3. Constitutive Model and Parameter Identification of Soft Soil Creep

3.1. Constitutive Model of Soft Soil Creep

Soft clay has poor engineering properties, and as the above tests show, it exhibits strong creep characteristics. Deformation is highly dependent on stress and time, and large deformations are prone to occur during construction. Therefore, to analyze the creep characteristics of soft clay, a soft soil creep constitutive model is established to improve the accuracy of subsequent engineering stability assessments. Based on the triaxial creep tests of soft clay mentioned above, soft soil creep is an instantaneous deformation, exhibiting a nonlinear elastic deformation law. Under relatively small loads, soft soil creep exhibits a creep decay stage and a stable creep stage; under larger loads, as time increases and the load exceeds a critical value, soft soil creep exhibits an accelerated creep stage. Therefore, the Burgers model is used to describe the creep deformation law of soft soil materials. However, because the Burgers model is a linear viscoelastic model, and soft soil creep exhibits an accelerated creep stage, it is modified accordingly.

The Burgers model is a viscoelastic model consisting of Maxwell bodies and Kelvin bodies connected in series, as shown in Figure 7, where $\mathrm{Bu} = \mathrm{M} - \mathrm{K}$. Therefore, the Burgers model satisfies the following constitutive relation:

$$\varepsilon = \varepsilon_1 + \varepsilon_2 \tag{1}$$

$$\sigma = \sigma_1 = \sigma_2 = \sigma_0 \tag{2}$$

$$\varepsilon = \left\{ \frac{1}{E_1} + \frac{1}{\eta_1} t + \frac{[1 - \exp(-\frac{E_2}{\eta_2} t)]}{E_2} \right\} \sigma \tag{3}$$

where ε is the total strain, σ_1 and ε_1 are the stress and strain of the Maxwell body, σ_2 and ε_2 are the stress and strain of the Kelvin body, σ_0 is the strain constant, E_1 and η_1 are the elastic modulus and viscosity coefficient of the Maxwell body, and E_2 and η_2 are the elastic modulus and viscosity coefficient of the Kelvin body.

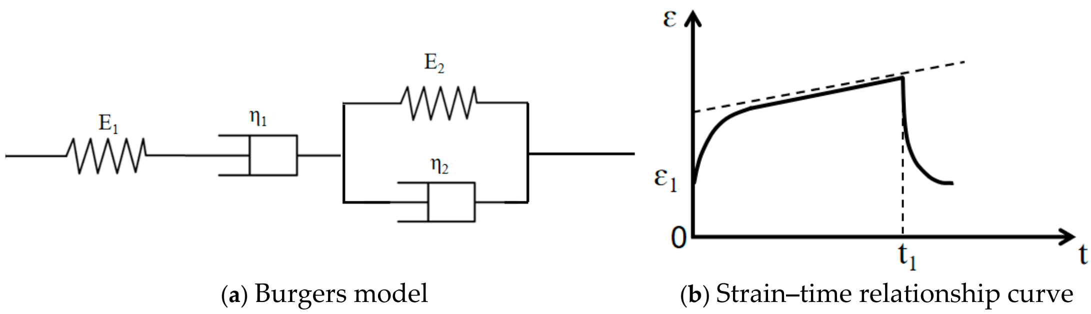

Figure 7. Burgers model and deformation characteristics.

In order to accurately simulate the instantaneous creep, attenuated creep, and stable creep stages of rock and soil materials, the viscosity coefficient η_1 of the Maxwell body in the Burgers model is unsteady, and η_1 decays with time. As can be seen from the above, the model of the viscous element is $\sigma = \eta \cdot \dot{\varepsilon}$. Therefore, it is assumed that η_1 satisfies the power-law decay [24]:

$$\eta_1(t) = \eta_1 \cdot \frac{1}{b_1} e^{b_1 t} \tag{4}$$

where η_1 and b_1 are constant coefficients.

Therefore, the Maxwell body creep constitutive model is

$$\varepsilon_1 = \frac{\sigma_0}{E_1} + \frac{\sigma_0}{\eta_1}(\varepsilon_{01} - e^{-b_1 t}) \tag{5}$$

where σ_0 is the strain constant. Because of the initial conditions $t = 0$, $\varepsilon_1 = 0$, we can obtain $\varepsilon_{01} = 1$.

Therefore, the undetermined creep constitutive equation of the Maxwell body can be written as

$$\varepsilon_1 = \frac{\sigma_0}{E_1} + \frac{\sigma_0}{\eta_1}(1 - e^{-b_1 t}) \tag{6}$$

Therefore, the constitutive equation of the Burgers model after improving the viscosity coefficient in the Maxwell volume is

$$\varepsilon = \{\frac{1}{E_1} + \frac{1}{\eta_1}(1 - e^{-b_1 t}) + \frac{[1 - \exp(-\frac{E_2}{\eta_2} t)]}{E_2}\}\sigma_0 \tag{7}$$

The above-mentioned improvement can simulate the instantaneous creep stage, attenuated creep stage, and stable creep stage of soft clay creep well. In order to describe the accelerated creep stage, the Burgers model is further improved. In order to realize the nonlinearity of viscous elements, the viscosity coefficient in the model is improved by using the principle of loss variable.

The model equation of the nonlinear viscous element is

$$\sigma = \eta(t) \cdot \dot{\varepsilon} = \eta_0 e^{-bt} \cdot \dot{\varepsilon} \tag{8}$$

Differentiating the viscosity coefficient above, we obtain

$$\dot{\eta}(t) = -b\eta_0 e^{-bt} \tag{9}$$

The viscosity coefficient is positive, thus obtaining

$$\begin{cases} \dot{\eta}(t) \leq 0, b > 0 \\ \dot{\eta}(t) = 0, b = 0 \\ \dot{\eta}(t) > 0, b < 0 \end{cases} \tag{10}$$

Based on the improved viscosity coefficient described above, the Kelvin bulk viscosity coefficient $\eta_2(t)$ is

$$\eta_2(t) = \eta_2^0 e^{-b_2 t} \tag{11}$$

In the formula, η_2^0 is the initial viscosity coefficient of Kelvin volume, and b_2 is a constant coefficient.

If the above conditions are met, b can change the properties of the nonlinear viscous element and also satisfy the condition of damage and hardening coexisting in the creep process [25,26].

Let the creep compliance of the elastic element in the Maxwell body be C_1, the creep compliance of the viscous element be C_2, and the creep compliance of the viscous element in the Kelvin body be C_3. The expression for C_1 is

$$C_1 = \frac{1}{E_1} \tag{12}$$

The expression for C_2 is

$$C_2 = \frac{1}{\eta_1}(1 - e^{-b_1 t}) \tag{13}$$

After separating the variables and taking the definite integral of the Kelvin model equation, the expression for C_3 is

$$C_3 = \frac{1 - \exp[-\frac{E_2}{b_2 \eta_2^0}(e^{b_2 t} - 1)]}{E_2} \tag{14}$$

Therefore, the creep constitutive equation of the improved Burgers model is

$$\varepsilon(t) = (C_1 + C_2 + C_3) \cdot \sigma_0 = \{\frac{1}{E_1} + \frac{1}{\eta_1}(1 - e^{-b_1 t}) + \frac{1 - \exp[-\frac{E_2}{b_2 \eta_2^0}(e^{b_2 t} - 1)]}{E_2}\}\sigma_0 \tag{15}$$

Express the three-dimensional creep constitutive equation of soft soil using stress components $\boldsymbol{\sigma}_{ij}$ and strain tensor $\boldsymbol{\varepsilon}_{ij}$. Under the action of three-dimensional stress, the expression [27] is generally

$$\begin{cases} \boldsymbol{\sigma}_{ij} = \boldsymbol{S}_{ij} + \delta_{ij}\boldsymbol{\sigma}_m \\ \boldsymbol{\varepsilon}_{ij} = \boldsymbol{e}_{ij} + \delta_{ij}\varepsilon_m \end{cases} \tag{16}$$

where the spherical stress tensor and the spherical strain tensor are $\begin{cases} \boldsymbol{\sigma}_m = \frac{\sigma_1 + \sigma_2 + \sigma_3}{3} \\ \boldsymbol{\varepsilon}_m = \frac{\varepsilon_1 + \varepsilon_2 + \varepsilon_3}{3} \end{cases}$; moreover, the elastic element under three-dimensional stress satisfies the generalized Hooke's law, that is, $\begin{cases} \boldsymbol{S}_{ij} = 2\boldsymbol{G}\boldsymbol{e}_{ij} \\ \boldsymbol{\sigma}_m = 3\boldsymbol{K}\boldsymbol{\varepsilon}_m \end{cases}$. Among them, $\boldsymbol{S}_{\mathrm{ij}}$ is the bias stress tensor, $\boldsymbol{e}_{\mathrm{ij}}$ is the bias strain tensor, G is the shear modulus, and K is the bulk modulus.

By substituting Equation (16) into Equations (7) and (15), the creep constitutive equation of the improved Burgers model under equal confining pressure conditions is obtained as follows:

$$\varepsilon(t) = \frac{\sigma_1 + 2\sigma_3}{9K} + \frac{\sigma_1 - \sigma_3}{3G_1} + \frac{\sigma_1 - \sigma_3}{3\eta_1}(1 - e^{-b_1 t}) + \frac{\sigma_1 - \sigma_3}{3G_2} \cdot [1 - e^{(-\frac{G_2}{\eta_2} t)}] \tag{17}$$

$$\varepsilon(t) = \frac{\sigma_1 + 2\sigma_3}{9K} + \frac{\sigma_1 - \sigma_3}{3G_1} + \frac{\sigma_1 - \sigma_3}{3\eta_1}(1 - e^{-b_1 t}) + \frac{\sigma_1 - \sigma_3}{3G_2} \cdot \{1 - e^{[-\frac{G_2}{b_2 \eta_2^0}(e^{b_2 t} - 1)]}\} \tag{18}$$

Among them, Equation (17) is used to describe the instantaneous creep stage, decay creep stage, and steady creep stage of soft soil material creep, and Equation (18) is used to describe the instantaneous creep stage, decay creep stage, steady creep stage, and accelerated creep stage of soft soil material creep.

3.2. Identification of Soft Soil Creep Model Parameters

At present, the most commonly used curve fitting method is the least square method, but for nonlinear solutions, its initial value selection is difficult, the convergence rate is slow, and it is easy to converge to local minima. Therefore, in order to overcome the above defects, the Levenberg–Marquardt algorithm is used to fit the creep test curve and identify the parameters. The soft soil creep constitutive model described by Equations (17) and (18) consists of many physical and mechanical parameters. In order to simplify the internal parameters of the formula, the constant terms in the two formulas are combined together, which can be obtained by fitting the creep curve through the experiment, as shown in the following formula:

$$A = \frac{\sigma_1 + 2\sigma_3}{9K} + \frac{\sigma_1 - \sigma_3}{3G_1} \tag{19}$$

Since G is the shear modulus and K is the bulk modulus, the formula for solving it is $\begin{cases} G = \frac{E}{2(1+\nu)} \\ K = \frac{E}{3(1-2\nu)} \end{cases}$, where E is the elastic modulus, and ν is Poisson's ratio, which is obtained from the above tests.

The model parameters of the creep test curve are determined according to the results of the soft soil triaxial creep test, as shown in Table 4.

Table 4. Fitting parameters for improved Burgers creep model.

Number	Improve Burgers Model Parameters							
	K/MPa	**G_1/MPa**	**η_1 /MPa·h**	**b_1**	**G_2 /MPa**	**b_2**	**η_2 /MPa·h**	**R^2**
A1	826.6	336.5	1227.1	0.070	602.1	/	198.6	0.97
A2	942.3	385.7	1306.9	0.064	849.3	/	214.8	0.98
A3	1223.5	374.1	397.6	−0.155	753.6	−0.674	253.7	0.98
B1	868.3	345.5	1275.1	0.072	623.4	/	201.3	0.97
B2	972.4	387.6	1417.5	0.073	856.1	/	223.9	0.96
B3	1246.1	377.7	383.2	−0.107	766.8	−0.633	286.7	0.97
C1	835.7	338.9	1053.6	0.068	608.7	/	184.4	0.98
C2	956.4	378.3	1309.8	0.063	786.9	/	211.2	0.98

As shown in Table 4, the determination coefficients of the parameters obtained from the fitting curve of the improved Burgers model are all above 0.9, indicating that the improved Burgers model has a high degree of fit and is correct. The model parameters b_1 and b_2 are positive in most cases, which indicates that the Kevin body in the constitutive model has the characteristic of hardening and weakens with the increase in stress. Under the action of high stress, the negative value shows that the damage deterioration of the soil sample increases suddenly when it reaches the failure stress, but it is not obvious under the low-stress condition. As shown in Figure 8, by improving the Burgers model and introducing the viscosity coefficient related to stress and strain, the whole process from attenuated creep to stable creep and then to accelerated creep can be simulated, in which the nonlinear damper ($\eta(t)$ variable) is the key, and then the linear and nonlinear parameters are determined, respectively, by the step loading creep test. Therefore, the improved Burgers model can better simulate the instantaneous creep stage, decay creep stage, steady creep stage, and accelerated creep stage of soft soil and can be applied to practical engineering. Looking at the comparison diagram between the improved unsteady Burgers model and the experiment, it can be seen that the nonlinear Burgers creep model of soft soil proposed in this paper can accurately simulate the relationship of the creep stages of soft soil and has strong applicability.

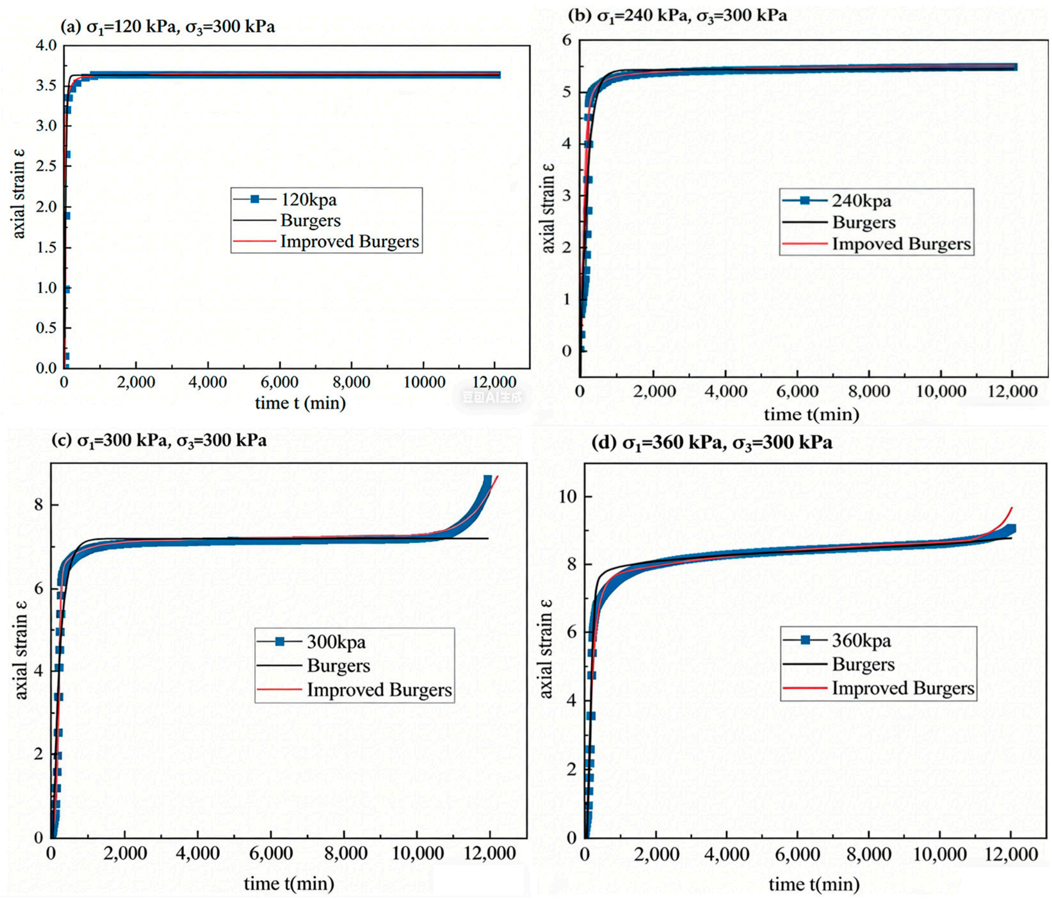

Figure 8. Creep test fitting curve.

In order to make the improved nonlinear Burgers creep constitutive model mentioned above possible for the secondary development of the FLAC3D software program, the finite split form of the improved creep constitutive relationship under three-dimensional stress state is rewritten. The improved creep constitutive of soil is embedded with the secondary development interface of the software, and the numerical simulation of the indoor triaxial creep test model is carried out to verify the accuracy of the secondary development of the model.

4. Secondary Development of FLAC3D Nonlinear Burgers Model

4.1. FLAC3D Finite Difference Forma

FLAC3D software contains a variety of constitutive models. Compared with the "discrete integration method" in finite element calculation software, it uses a hybrid discretization method to fit soil deformation, making the calculation results more accurate [28]. FLAC3D software supports the numerical analysis of custom constitutive models, which are written as "dynamic link libraries" and embedded in the model library and called by the main program of the software. The prerequisite for satisfying the secondary development of creep constitutive models is to first perform finite difference derivation on the custom creep constitutive models, rewrite the stress and strain increments in the creep constitutive relationship derivation into time-related difference forms, and establish the incremental relationship of total soil strain, instantaneous elastic body, viscoelastic body, nonlinear viscous body, etc., in one time step.

In the Burgers creep constitutive model, the elements are in series, and the total strain is equal to the sum of the strains of each element, as shown in Equation (20).

$$\boldsymbol{\varepsilon}_{ij} = \boldsymbol{\varepsilon}_{ij}^1 + \boldsymbol{\varepsilon}_{ij}^2 + \boldsymbol{\varepsilon}_{ij}^3 \tag{20}$$

Then, the deviatoric strain rate is written as

$$e_{ij} = e_{ij}^1 + e_{ij}^2 + e_{ij}^3 \tag{21}$$

Therefore, the total strain increment of the entire model within one time step is

$$\Delta e_{ij} = \Delta e_{ij}^1 + \Delta e_{ij}^2 + \Delta e_{ij}^3 \tag{22}$$

The three-dimensional difference form in the custom creep constitutive relationship is to rewrite the element formula into an incremental difference form with respect to time t, which can be expressed as

$$\begin{aligned} &\Delta e_{ij}^1 = \frac{\Delta S_{ij}}{2G_1} \\ &\Delta e_{ij}^2 = \frac{\Delta S_{ij} \cdot (1 - e^{-b_1 \Delta t})}{2\eta_1} \\ &\overline{S}_{ij} \Delta t = 2G_2 \overline{e}_{ij}^3 \Delta t + 2\eta_2 \Delta e_{ij}^3 \Delta t \\ &\overline{S}'_{ij} \Delta t = 2G_2 \overline{e}'^3_{ij} \Delta t + 2b_2 \eta_2 \Delta e'^3_{ij} \cdot \frac{1}{(e^{b_2 \Delta t} - 1)} \end{aligned} \tag{23}$$

where

$$\begin{aligned} &\Delta e_{ij}^1 = e_{ij}^{1,N} - e_{ij}^{1,O} \\ &\Delta e_{ij}^2 = e_{ij}^{2,N} - e_{ij}^{2,O} \\ &\Delta e_{ij}^3 = e_{ij}^{3,N} - e_{ij}^{3,O} \\ &\overline{e}_{ij}^3 = \frac{e_{ij}^{3,N} + e_{ij}^{3,O}}{2} \end{aligned} \tag{24}$$

$$\begin{aligned} &\Delta S_{ij} = S_{ij}^N - S_{ij}^O \\ &\overline{S}_{ij} = \frac{S_{ij}^N + S_{ij}^O}{2} \\ &\overline{S}'_{ij} = \frac{S'^N_{ij} + S'^O_{ij}}{2} \end{aligned} \tag{25}$$

In the formula, e_{ij}^N, e_{ij}^O denote the new and old bias strains in a time step, and S_{ij}^N, S_{ij}^N denote the new and old bias stresses in a time step.

Substituting Equations (24) and (25) into Equation (23), we can obtain

$$\begin{aligned} \frac{S_{ij}^{N}+S_{ij}^{O}}{2}\cdot\Delta t &= G_2\cdot(e_{ij}^{3,N}+e_{ij}^{3,O})\cdot\Delta t+2\eta_2\cdot(e_{ij}^{3,N}-e_{ij}^{3,O})\cdot\Delta t \\ \frac{S_{ij}^{\prime N}+S_{ij}^{\prime O}}{2}\Delta t &= G_2\cdot(e_{ij}^{3,N}+e_{ij}^{3,O})\cdot\Delta t+2b_2\eta_2\cdot(e_{ij}^{3,N}-e_{ij}^{3,O})\cdot\frac{1}{(e^{b_2\Delta t}-1)} \end{aligned} \tag{26}$$

From the above equation, we can obtain

$$\begin{aligned} e_{ij}^{3,N} &= \frac{1}{G_2\Delta t+2\eta_2}\cdot[\frac{\Delta t}{2}(S_{ij}^{N}+S_{ij}^{O})+(2\eta_2-G_2\Delta t)\cdot e_{ij}^{3,O}] \\ e_{ij}^{\prime 3,N} &= \frac{1}{G_2\Delta t+2\eta_2}\cdot[\frac{\Delta t}{2}(S_{ij}^{\prime N}+S_{ij}^{\prime O})+(\frac{2b_2\eta_2}{e^{b_2\Delta t}-1}-G_2\Delta t)\cdot e_{ij}^{3,O}] \end{aligned} \tag{27}$$

Let $A=1+\frac{G_2\Delta t}{2\eta_2}$, $B=1-\frac{G_2\Delta t}{2\eta_2}$ be reduced to

$$\begin{aligned} e_{ij}^{3,N} &= \frac{1}{A}\cdot[\frac{\Delta t}{4\eta_2}(S_{ij}^{N}+S_{ij}^{O})+B\cdot e_{ij}^{3,O}] \\ e_{ij}^{\prime 3,N} &= \frac{1}{A}\cdot[\frac{\Delta t}{4\eta_2}(S_{ij}^{\prime N}+S_{ij}^{\prime O})+(B+\frac{b_2}{e^{b_2\Delta t}-1}-1)\cdot e_{ij}^{3,O}] \end{aligned} \tag{28}$$

Therefore, the total strain increment of the creep model is

$$\begin{aligned} \Delta e_{ij} &= \frac{\Delta S_{ij}}{2G_1}+\frac{\Delta S_{ij}\cdot(1-e^{-b_1\Delta t})}{2\eta_1}+\frac{1}{A}\cdot[\frac{\Delta t}{4\eta_2}(S_{ij}^{N}+S_{ij}^{O})+B\cdot e_{ij}^{3,O}]-e_{ij}^{3,O} \\ \Delta e_{ij}^{\prime} &= \frac{\Delta S_{ij}}{2G_1}+\frac{\Delta S_{ij}\cdot(1-e^{-b_1\Delta t})}{2\eta_1}+\frac{1}{A}\cdot[\frac{\Delta t}{4\eta_2}(S_{ij}^{N}+S_{ij}^{O})+(B+\frac{b_2}{e^{b_2\Delta t}-1}-1)\cdot e_{ij}^{\prime 3,O}]-e_{ij}^{\prime 3,O} \end{aligned} \tag{29}$$

From the above equation, the three-dimensional finite difference scheme of the custom creep constitutive model can be obtained:

$$\begin{aligned} S_{ij}^{N} &= \frac{1}{X}[\Delta e_{ij}+YS_{ij}^{o}-(\frac{B}{A}-1)\cdot e_{ij}^{3,o}] \\ S_{ij}^{\prime N} &= \frac{1}{X}[\Delta e_{ij}+YS_{ij}^{o}-(\frac{B}{A}+\frac{1}{A}\cdot\frac{b^2}{e^{b_2\Delta t}-1}-1)\cdot e_{ij}^{3,o}] \end{aligned} \tag{30}$$

where

$$\begin{aligned} X &= \frac{1}{2G_2}+\frac{1-e^{-b_1\Delta t}}{2\eta_1}+\frac{\Delta t}{4A\eta_2} \\ Y &= \frac{1}{2G_2}+\frac{1-e^{-b_1\Delta t}}{2\eta_1}-\frac{\Delta t}{4A\eta_2} \end{aligned} \tag{31}$$

4.2. Secondary Development Process of Creep Model

The development of the custom creep constitutive model was completed in the Microsoft Visual Studio 2019 Community (VS 2019) environment. The decomposition relationship of the above 3D creep constitutive model was written into the software to complete the secondary development of the FLAC3D software. The specific development steps are as follows:

(1) In FLAC3D, locate the headfiles folder in the installation directory. This folder contains all necessary header files. Create a new C++ Dynamic-Link Library (DLL) project in VS 2019 and compile it into a Dynamic-Link Library so that it can be called in the software.
(2) Modify the header file (.h file), rename the header file, and modify the parameters and key variables in the creep model description.
(3) Modify the source file (.cpp file), rename the source file, change the custom model to the central difference format, and modify the Initialize(), Properties(), and Run() functions, etc.
(4) Generate the .dll file, place it in the Itasca\models folder in the FLAC3D software, load the model, and enter the udm command to load the model into the software.

The second development mainly includes five parts, which are as follows: defining the base class function, registering the model, data transfer between the type and the main program, and describing the status indicator. The key step is to obtain a new stress increment from the existing strain increment, which is realized by modifying the source file (.cpp). The two most important functions when modifying the source file are the Initialize() and Run() functions. Among them, the Initialize() function initializes common variables and variables generated in calculations. In order to ensure the stability of the model, it is necessary to check the elastic modulus of the elements, which should not be less than 0. In order to complete the realization from the strain increment to stress increment, the Run() function needs to be called in each cycle, and the implicit renewal mode is adopted. After the material enters the yield, the stress–strain relationship is nonlinear, and the solution for the stress increment needs to be obtained through repeated iterations of the strain increment. Among them, the maximum creep strain increment is controlled to adapt to the time step. In order to reduce the amount of computation, large-scale looping statements should be avoided as much as possible.

4.3. Indoor Triaxial Test Model Verification

To ensure the correctness of the secondary development of the custom creep constitutive model presented in this paper, a numerical model identical to that used in the indoor creep test was established using FLAC3D software to verify its accuracy. The model parameters and dimensions were consistent with the experimental parameters, being a 50 mm × 100 mm cylinder, divided into 17,280 elements and 17,887 nodes. Uniform vertical stress needs to be applied at the top of the model, constant confining stress (simulated confining pressure) needs to be applied around the model, and boundary constraints are set at the bottom in the vertical direction. The test conditions were conducted using silty clay 1, with an axial compressive pressure of 300 kPa and a confining pressure of 300 kPa. The triaxial creep test numerical model is shown in Figure 9.

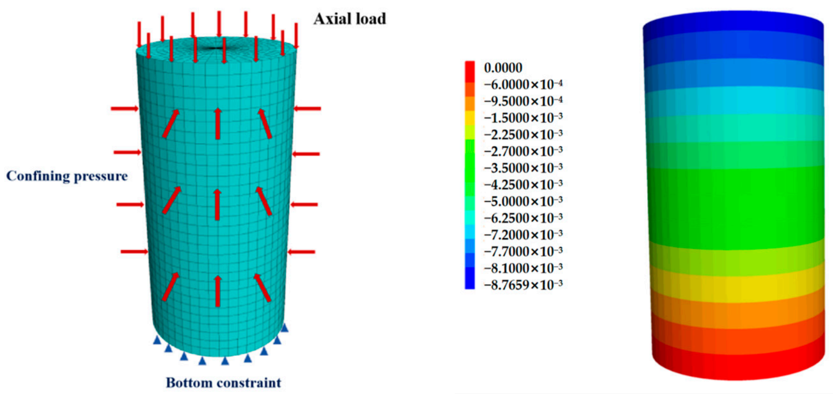

Figure 9. Indoor three-axis numerical simulation strain cloud.

As can be seen from Figure 10, the determination coefficient R^2 between the numerical model and the laboratory test data of the muddy silty clay 2 under the axial compression of 100 kPa and confining pressure of 120 kPa and the muddy silty clay 1 under the axial compression of 300 kPa and confining pressure of 300 kPa are both above 0.9, indicating that the fitting accuracy is high. The self-defined creep constitutive model is good for the instantaneous creep, attenuated creep, and stable creep of soft soil under low stress. Similarly, it can also simulate the instantaneous creep, attenuated creep, stable creep, and accelerated creep of soft soil under high stress, especially the instantaneous creep and accelerated creep. It can be seen from the figure that the axial displacement of the muddy silty clay 1 sample gradually decreases from the top, and the maximum displacement of the numerical simulation is 8.7659 mm, while the data for the indoor creep test is 8.5812 mm. The difference between the two is very small, which fully demonstrates the adaptability of the custom creep constitutive model in the FLAC3D software. The test results can be applied to general water-rich soft soil and can provide a basis for the research and analysis of corresponding soil engineering construction.

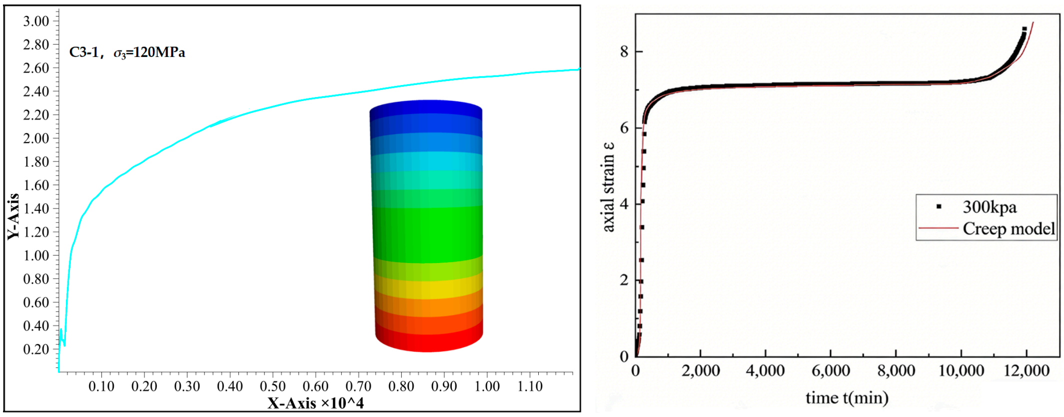

Figure 10. Creep test verification.

5. Conclusions

Through indoor tests, the creep test data of soft soil were analyzed to reveal the creep deformation law of soft soil materials. By performing unsteady processing on the parameters, an improved unsteady Burgers creep model was constructed, and its parameters were inverted. Furthermore, the nonlinear creep constitutive model was further developed based on FLAC3D. The specific research content is as follows:

(1) Undrained triaxial shear tests and triaxial creep tests were conducted on soft soil to obtain stress–strain curves and a cluster of creep-time curves. The tests revealed that soft soil samples exhibit a significant creep effect. Under low to medium stress levels, soft soil creep exhibits attenuating creep characteristics, while under high stress levels, it exhibits non-attenuating creep characteristics. Furthermore, soft soil creep is nonlinear creep; during loading, the deformation rate of the soil sample is initially rapid and then tends to stabilize. The applied deviatoric stress, confining pressure, and time in soft soil creep are all positively correlated with the nonlinear deformation.

(2) Considering the negative exponential relationship between soil creep parameters and time, the two viscous elements in the traditional Burgers model are nonlinearly processed to establish an improved unsteady Burgers model, deriving a one-dimensional creep constitutive equation, which is then transformed into a three-dimensional creep constitutive equation. The improved unsteady Burgers model is validated using experimental data, and parameter fitting and identification are performed. The established, improved Burgers creep model can effectively simulate the entire process of soil samples during the experiment.

(3) The unsteady Burgers creep constitutive equation is transformed under the three-dimensional stress state. Based on FLAC3D software and combined with the fitted data, a secondary development of the nonlinear creep constitutive model is completed. The applicability and correctness of the custom creep constitutive model are verified using a cylindrical test body. The results show that the numerical model data fits the experimental data well, and the custom creep model is effective.

Author Contributions: All authors contributed to the study's conception and design. Conceptualization was performed by R.Z. and B.W. Data collection was performed by R.Z. Formal analysis was performed by R.Z. Investigation was performed by R.Z. and S.X. Methodology was performed by

B.W. Writing—original draft was performed by R.Z. Project administration was performed by B.W., X.L., and H.L. All authors have read and agreed to the published version of the manuscript.

Funding: This APC was funded by the Natural Science Foundation of China (Grant Numbers: 52168055 and 52278397), the Natural Science Foundation of Jiangxi Province (Grant Number: 20212ACB204001), "Double Thousand Plan" Innovation Leading Talent Project of Jiangxi Province (Grant Number: jxsq2020101001), China Postdoctoral Science Foundation (Grant Number: 2022M711429), Natural Science Foundation of Jiangxi Province (Grant Number: 20224BAB204058), the Open Foundation of MOE Key Laboratory of Engineering Structures of Heavy Haul Railway (Central South University) (Grant Number: 2022JZZ01), and the Jiangxi Province Graduate Innovation Special Fund Project (Grant Number: YC2022-B179). Their support is gratefully acknowledged.

Institutional Review Board Statement: Not applicable.

Informed Consent Statement: Not applicable.

Data Availability Statement: The datasets generated and analyzed during the current study are not publicly available but are available from the corresponding author upon reasonable request.

Conflicts of Interest: Author Xi Liu and Heshan Li were employed by the China Tielong Engineering Group Co., Ltd. The remaining authors declare that the research was conducted in the absence of any commercial or financial relationships that could be construed as a potential conflict of interest.

References

1. Deng, X.; He, H.; Wang, R.; Zhang, X.; Zhao, B.; Ding, X. Study on the optimization of the inclination angle of the locking anchor pipe in the excavation of the upper and middle steps of the deep buried soft rock tunnel. *Chin. J. Geotech. Eng.* **2024**, *47*, 1–11.
2. Zhang, L.-l.; Cheng, H.; Zhishu, Y.; Wang, X.-J. Prediction model for rock creep failure time under conventional triaxial compression. *Rock Soil Mech.* **2025**, *46*, 2011–2022.
3. Wang, R.; Zhang, Z.; Deng, X.; Huang, X.; Zhou, Y. Calculation Method for the Loose Circle of tunnel-surrounding rock considering the strain-softening effect. *Int. J. Geomech.* **2024**, *24*, 04024216. [CrossRef]
4. Sun, J. Rock Rheological Mechanics and its Advance in Engineering Applications. *Chin. J. Rock Mech. Eng.* **2007**, *26*, 1081–1106.
5. Qin, P.; Zheng, W.-J.; Xue, Z.-F.; Zhang, Y.-L.; Wang, L.; Li, J.; Ma, H. Study on Creep Characteristics of Straw Reinforced Loess and Modified Burgers Model. *Adv. Eng. Sci.* **2023**, *55*, 181–190.
6. Li, T.-G.; Tang, B.; Cheng, H.; Liu, X.-H.; Hou, J.-L.; Li, H.-L.; Wang, X.-Y. Creep mechanical characteristics of fractured rock mass in coal measure strata under anchoring conditions. *Rock Soil Mech.* **2024**, *45*, 1–10.
7. Khaledi, K.; Mahmoudi, E.; Datcheva, M.; König, D.; Schanz, T. Sensitivity analysis and parameter identification of a time dependent constitutive model for rock salt. *J. Comput. Appl. Math.* **2016**, *293*, 128–138. [CrossRef]
8. Zhu, Y.-G.; Wang, X.-Y.; Liu, B.; Liu, X.-W.; Xue, H.-Y.; Geng, Z. Transversely isotropic creep damage constitutive model for layered rocks. *Rock Soil Mech.* **2025**, *46*, 1095–1108.
9. Li, Y.L.; Yu, H.C.; Liu, H.D. Study of creep constitutive model of silty mudstone under triaxial compression. *Rock Soil Mech.* **2012**, *33*, 2035–2040. (In Chinese)
10. Zhao, B.Y.; Liu, D.Y.; Dong, Q. Experimental research on creep behaviors of sandstone under uniaxial compressive and tensile stresses. *J. Rock Mech. Geotech. Eng.* **2011**, *3*, 438–444.
11. Dongyan, L.; Baoyun, Z.; Keshan, Z.H.U.; Kaixi, X.U.E. Direct tension creep behaviors of sandstone and improvement and application of Burgers model. *Chin. J. Geotech. Eng.* **2011**, *33*, 1740–1744. (In Chinese)
12. Xue, K.; Zhao, B.; Liu, D.; Hu, Y.-X. Nonlinear creep model of rock in tensile or compressive stress and its parameter identification. *J. China Coal Soc.* **2011**, *36*, 1440–1445. (In Chinese)
13. Guan, Z.C.; Jiang, Y.J.; Tanabashi, Y.; Huang, H. A new rheological model and its application in mountain tunneling. *Tunn. Undergr. Space Technol.* **2008**, *23*, 292–299. [CrossRef]
14. Sterpi, D.; Gioda, G. Visco-plastic behaviour around advancing tunnels in squeezing rock. *Rock Mech. Rock Eng.* **2009**, *42*, 319–339. [CrossRef]
15. Fahimifar, A.; Karami, M.; Fahimifar, A. Modifications toan elasto-visco-plastic constitutive model for prediction of creep deformation of rock samples. *Soils Found.* **2015**, *55*, 1364–1371. [CrossRef]
16. Yin, Z.C.; Zhang, X.; Li, X.; Zhang, J.; Zhang, Q. Modified Burgers model of creep behavior of grouting-reinforced body and its long-term effect on tunnel operation. *Tunn. Undergr. Space Technol.* **2022**, *127*, 104537. [CrossRef]
17. Jang, H.P.; Jang, A.N. Numerical analysis and application of Nishihara creep nonlinear damage model considering ubiquitous joints. *Tunn. Undergr. Space Technol.* **2025**, *157*, 106335. [CrossRef]

18. Tang, Z.-Q.; Ji, F.; Xu, H.-H. Creep characteristics and nonlinear creep damage model of Yanshanian granite in southern Henan. *Sci. Technol. Eng.* **2022**, *22*, 6421–6429.
19. Li, Z.-J.; Sheng, D.-F.; Cheng, X.; Wang, Y. Study of nonlinear creep model for rocks considering time-dependent damage. *Chin. Q. Mech.* **2022**, *43*, 835–843.
20. Chen Lw Ls, I.; Zhang, K.X.; Liu, Y.X. Secondary development and application of the NP-T creep model based on FLAC3D. *Arab. J. Geosci.* **2017**, *10*, 1–11. [CrossRef]
21. Zhu, X.; Hu, B.; Li, J.; Cui, K.; Wei, E.; Liu, Y. Study on shear rheology constitutive model of weak interlayer considering damage and its program realization. *Hydro-Sci. Eng.* **2021**, *6*, 124–132.
22. *GB/T50123—2019*; Standard for Geotechnical Testing Methods. Planning Press: Beijing, China, 2019.
23. Lei, H.; Yang, C.; Liu, Z. Triaxial creep test of loess and correction of Singh-Mitchell model. *Hydropower Energy Sci.* **2015**, *33*, 112–115.
24. Zhou, J.; Xu, W.; Yang, S. Improved generalized Bingham rock creep model. *J. Hydraul. Eng.* **2006**, *37*, 827–830+837.
25. Fan, Q.; Gao, Y. Study on creep characteristics and nonlinear model of soft rock. *Chin. J. Rock Mech. Eng.* **2007**, *26*, 391–396.
26. Han, Y.; Tan, Y.; Li, E.; Duan, J.-L.; Pu, S.-K. Unsteady Burgers creep model of rock and its parameter identification. *Eng. Mech.* **2018**, *35*, 210–217.
27. Li, G. *Advanced Soil Mechanics*, 2nd ed.; Tsinghua University Press: Beijing, China, 2016; pp. 42–46.
28. Zou, W. Research on Dynamic Response Characteristics and Service Status Evaluation System of Heavy-Haul Railway Tunnel Foundation Structure. Ph.D. Thesis, China Academy of Railway Sciences, Beijing, China, 2016.